THE JOURNAL OF PHYSICAL CHEMISTRY Letters

pubs.acs.org/JPCL Letter

Charge Transfer in the Heterostructure of $CsPbBr_3$ Nanocrystals with Nitrogen-Doped Carbon Dots

Ekashmi Rathore, Krishnendu Maji, Dheemahi Rao, Bivas Saha, and Kanishka Biswas*

Cite This: J. Phys. Chem. Lett. 2020, 11, 8002–8007 Read Online

ACCESS | Metrics & More | Article Recommendations | Supporting Information

ABSTRACT: Heterostructures of inorganic halide perovskites with mixed-dimensional inorganic nanomaterials have shown great potential not only in the field of optoelectronic energy devices and photocatalysis but also for improving our fundamental understanding of the charge transfer across the heterostructure interface. Herein, we present for the first time the heterostructure integration of the $CsPbBr_3$ nanocrystal with an N-doped carbon dot. We explore the photoluminescence (PL) and photoconductivity of the heterostructure of $CsPbBr_3$ nanocrystals and N-doped carbon dots. PL quenching of $CsPbBr_3$ nanocrystals with the addition of N-doped carbon dots was observed. The photoexcited electrons from the conduction band of $CsPbBr_3$ are trapped in the N-acceptor state of N-doped carbon dots, and the charge transfer occurs via quasi type II-like electronic band alignment. The charge transfer in the halide perovskite-based heterostructure should motivate further research into the new heterostructure synthesis with perovskites and the fundamental understanding of the mechanism of charge/energy transfer across the heterostructure interface.

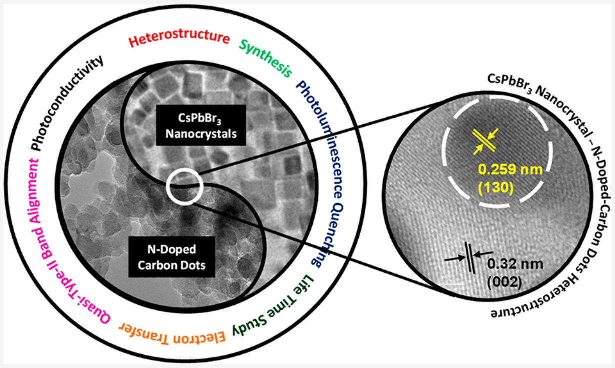

Recent advances in all-inorganic halide perovskites have created a sensation in diverse optoelectronic applications like photovoltaics, photodetectors, light-emitting diodes, and lasers.[1−10] The high absorption coefficient, wide absorption range, high photoluminescence quantum efficiencies (>90%), and long electron−hole diffusion lengths of halide perovskites make them attractive in these fields.[6−17] However, a diminution in dimensionality from bulk perovskites to nanocrystals [zero-dimensional (0D)] and other low-dimensional [one-dimensional (1D) and two-dimensional (2D)] structures has attracted more attention due to their tunable band gap, optoelectronic properties, etc.[18,19]

In parallel during the past decade, 2D materials like graphene, phosphorene, MoS_2, and MXenes have attracted significant attention in optoelectronics due to their layer-dependent electronic structure and their electronic band gap that can be tuned by doping.[20−25] Recently, mixed-dimensional nanoheterostructures of different inorganic compounds demonstrate great potential for the discovery of new materials and properties.[1,26−28] The optoelectronic properties, photoresponse, and efficient CO_2 reduction capability have been enhanced by the formation of heterostructures between 2D layered materials (graphene oxide, MXene, and phosphorene) and $CsPbBr_3$ nanocrystals (NCs).[29−33] The heterostructure of metal chalcogenide semiconductors like ZnS, CdS, CdSe, PbS, and PbSe with $CsPbBr_3$ and $CsPbI_3$ NCs exhibited type I or type II band alignments, which had a tremendous impact on tuning the photoresponsivity and luminescent properties.[34−38] However, the heterostructure integration of $CsPbBr_3$ nanocrystals with the 0D carbon dots has not yet been explored. 0D carbon dots (CDs) have unique electrical, optical, and chemical properties.[39−41] By doping with various elements (e.g., nitrogen, boron, or sulfur), one can modulate the optical properties of CDs.[42] Interestingly, N-doping in CDs produced electron-accepting trap states, which enhanced the charge separation as well as quantum efficiency.[43−47] Hence, N-doped CDs have attracted attention in diverse fields such as the electrocatalytic oxygen reduction reaction,[48] light-driven water splitting,[49] and photocatalysis.[50]

Herein, we have synthesized the heterostructure of $CsPbBr_3$ NCs with N-doped CDs and investigated the charge transfer between the two systems. $CsPbBr_3$ NCs were anchored on the N-doped CDs via H-bonding interactions of the $-NH_2$/−COOH group present in oleylamine/oleic acid ligands on the $CsPbBr_3$ surface with the functional groups (C═O, C−O, O−H, $-NH_2$, O═C−OH, etc.) on the N-doped CDs. N-Doping forms the trap states below the conduction band of the CDs. We noted momentous quenching of the photoluminescence of

Received: July 14, 2020
Accepted: September 1, 2020
Published: September 1, 2020

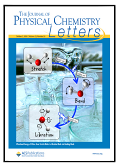

https://dx.doi.org/10.1021/acs.jpclett.0c02139
J. Phys. Chem. Lett. 2020, 11, 8002−8007

$CsPbBr_3$ within the heterostructure systems. To explore the mechanism of PL quenching in the heterostructure, we have carried out time-resolved PL spectroscopy and measured the photoconductivity of the $CsPbBr_3$−N-doped CD device. PL quenching occurs due to the transfer of an electron from the conduction band of the halide perovskite to the N-acceptor state of the N-doped CDs via a quasi type II electronic band alignment.

$CsPbBr_3$ NCs were synthesized by a solution-based hot-injection method with Cs oleate and $PbBr_2$ as precursors (see the Supporting Information).[3] The powder X-ray diffraction (PXRD) pattern of synthesized $CsPbBr_3$ NCs matched well with the simulated orthorhombic phase (*Pbnm*) (see Figure 1a). The nearly monodispersed square-shaped morphology of

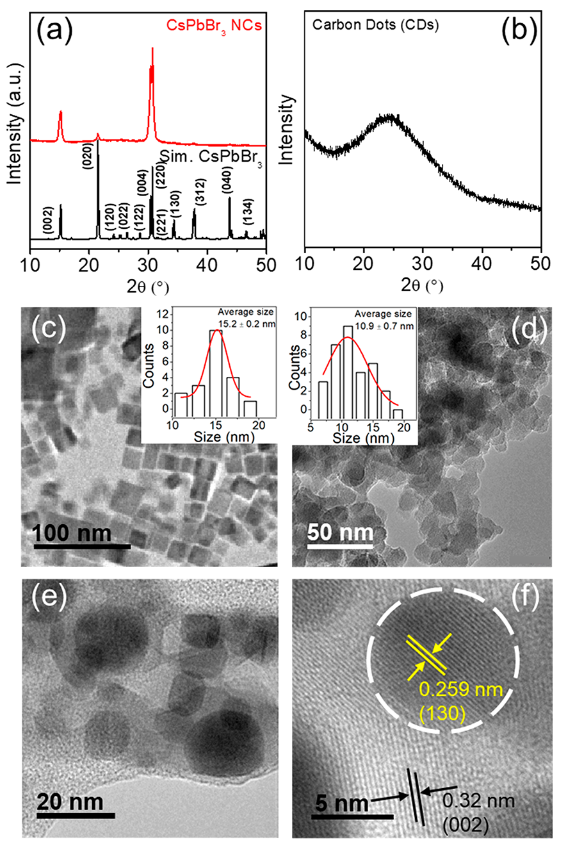

Figure 1. Powder X-ray diffraction (PXRD) and TEM images of (a and c) $CsPbBr_3$ nanocrystals (NCs) and (b and d) N-doped carbon dots (CDs), respectively. The inset shows the particle size distribution for $CsPbBr_3$ NCs and N-doped CDs, and the red line indicates Gaussian fitting. (e) TEM and (f) HRTEM images of the heterostructure of the $CsPbBr_3$ NC−N-doped CD system. The white circle (darker contrast) denotes $CsPbBr_3$ NCs with a 0.259 nm *d* spacing, and the light contrast region corresponds to N-doped CDs with a 0.32 nm *d* spacing.

$CsPbBr_3$ NCs with an average particle size of 15.2 nm can be visualized in the transmission electron microscopy (TEM) image (Figure 1c). These nanocrystals of $CsPbBr_3$ are well dispersed in toluene but unstable in water. To achieve successful heterostructure integration of $CsPbBr_3$NCs with 0D carbon dots, the challenge was to select a suitable common solvent as carbon dots can usually be dispersed in aqueous medium.

Hence, we have synthesized N-doped carbon dots (CDs) with controlled amino-passivated surfaces, which could be dispersed in toluene, as well. The N-doped CDs were synthesized by using a hydrothermal reaction with citric acid and urea as precursors (see the detailed synthesis in the Supporting Information). The product of the hydrothermal reaction was centrifuged at 9000 rpm to remove the larger particles. Then, the dispersion solution was dialyzed against distilled water for 24 h. At the end, the final dispersed solution was vacuum-dried. The PXRD patterns of CD samples show a broad peak centered at 24.5° (Figure 1b), indicating disordered graphitic layers [i.e., (002) planes] in the CDs.[45] In the Fourier transform infrared spectroscopy (FTIR) spectrum (Figure S1a), the intensity of the N−H peak at 1572 cm^{-1} is stronger than that of the C═O peak at 1698 cm^{-1}, signifying that the synthesized CDs have more amino groups on their surface.[44] The XPS peaks at 398.2 and 399.4 eV for N 1s shown in Figures S2a and S3c reveal that nitrogen presents as $(C)_3$−N (sp^3) and N−H (sp^3), respectively, which confirms the N-doping in CDs. The N-doped CDs were found to exist as clusters and have a nearly uniform size distribution with an average diameter of 10.9 nm (see the TEM image in Figure 1d).

To form the heterostructures between $CsPbBr_3$ NCs and N-doped CDs, the toluene-dispersed N-doped CDs with different concentrations were added to the $CsPbBr_3$ solution in toluene and the mixture was sonicated at room temperature to induce anchoring of $CsPbBr_3$ NCs with N-doped CDs. PXRD of the integrated heterostructure shows the presence of both $CsPbBr_3$ NCs and N-doped CDs (Figure S4). The assembly of $CsPbBr_3$ NCs on N-doped CDs can also be seen from the TEM image (Figure 1e). The high-resolution TEM (HRTEM) image of the heterostructure shows the (130) lattice planes of $CsPbBr_3$ NCs with an interplanar distance of 0.259 nm, and (002) graphitic planes with a 0.32 nm distance for N-doped CDs (Figure 1f). In addition, we have measured the FTIR spectra of pure $CsPbBr_3$ NCs and the heterostructure of the $CsPbBr_3$ NC−N-doped CD system (Figure S1b,c). The FTIR of $CsPbBr_3$ NCs is dominated mainly by the ν_{C-H} (~3000 cm^{-1}), $\nu_{C=O}$ (~1715 cm^{-1}), ν_{N-H} (~3139 cm^{-1}), and ν_{COO-} (~1407 cm^{-1}) modes of oleylamine and oleic acid (Figure S1b).[51−53] Formation of the heterostructures between $CsPbBr_3$ NCs and N-doped CDs is possibly due to the H-bonding interactions of the $-NH_2$/−COOH group present in oleylamine/oleic acid capping ligands on the surface of $CsPbBr_3$ NCs with the functional groups (C═O, C−O, O−H, $-NH_2$, O═C−OH, etc.) of N-doped CDs. The characteristic shift of the $\nu_{C=O}$ mode from oleic acid on $CsPbBr_3$ NCs (1713 cm^{-1}) to a lower wavenumber of 1706 cm^{-1} in the $CsPbBr_3$−N-doped CD heterostructure along with the mode broadening implies the possible H-bonding interaction in the heterostructures (Figure S1c). We also performed XPS on $CsPbBr_3$ and the $CsPbBr_3$−N-doped CD heterostructure, and the results are presented in Figures S2, S3, and S5. In Figure S3b, we show a slight shift in the C−O peak for O 1s from 531.0 eV for pure N-doped CDs to 530.7 eV for the heterostructure. For N 1s, the N−H peak shifts from 399.4 eV for pure N-doped CDs to 398.95 eV for the heterostructure (Figure S3c). These slightly smaller shifts in binding energy are indicative of H-bonding interaction being present in the heterostructure.[54]

To visualize further the interaction between the $CsPbBr_3$ and N-doped CDs, first the optical properties of N-doped CDs were studied using ultraviolet−visible (UV−vis) absorption and photoluminescence (PL) spectroscopy (see Figure 2). In the electronic absorbance spectrum of N-doped CDs in an

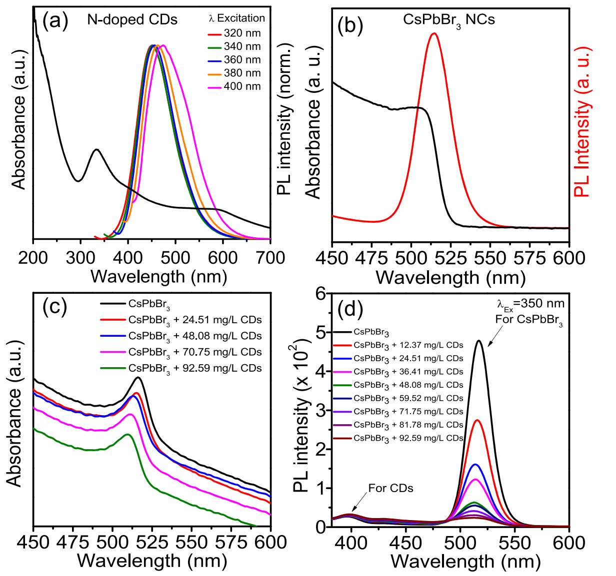

Figure 2. UV−vis absorption (black) and PL spectra (color) of (a) N-doped CDs in aqueous medium and (b) $CsPbBr_3$ NCs in a toluene medium. (c) UV−vis absorption and (d) PL spectra of the $CsPbBr_3$ NC−N-doped CD heterostructure system with variable concentrations of carbon dots (12.37−92.59 mg/L) in 1.97×10^{-6} M $CsPbBr_3$NCs in toluene.

aqueous solution, we observed an sp^2 carbon network band at ∼220 nm ($\pi-\pi^*$ transition), an absorbance band in the range of 325−400 nm corresponding to the $n-\pi^*$ transition of C═O, and a shoulder band in the range of 550−620 nm attributed to the $n-\pi^*$ transition of C═N arising from functional groups present on the surface of N-doped CDs (Figure 2a).[47,55] PL spectra of N-doped CDs slightly vary with excitation wavelength (from 320 to 400 nm), in which the emission maximum is red-shifted with an increase in the excitation wavelength (Figure 2a).[39,40,56,57] In addition, the peak width of PL emission increases with an increase in excitation wavelength (Figure S6a), which is attributed to the activation of trap states.[58] The N-doping leads to electron-trapping N-surface states in CDs (below the conduction band), which increases the high yield of radiative recombination.[44,55] Figure 2b shows absorption and PL spectra of $CsPbBr_3$ NCs with an absorption band peak at 507 nm and band edge emission at 517 nm. The absorption edges estimated from Tauc plots of the absorption data taken in toluene medium are 2.32, 3.65, and 4.15 eV for N-doped CDs and 2.37 eV for $CsPbBr_3$ (Figure S6b−d).

Electronic absorbance and PL spectra of $CsPbBr_3$ NCs with different concentrations of N-doped CDs in toluene are shown in panels c and d of Figure 2, respectively. The concentration of $CsPbBr_3$ (1.97×10^{-6} M) is kept constant, and a different concentration of N-doped CDs is added. The absorbance retained the feature of $CsPbBr_3$ NCs with the successive addition of N-doped CDs, while the PL intensity gradually decreased with a slight blue shift. The formation of the $CsPbBr_3$ heterostructure with N-doped CDs leads to the quenching of PL and may be attributed to the transfer of photogenerated carriers between them. A maximum PL quenching efficiency of ∼95% was achieved when 92.59 mg of N-doped CDs per liter was added to a 1.97×10^{-6} M $CsPbBr_3$ solution.

The nature of the quenching process that leads to the decrease in PL intensity in general can be governed by various factors like collision (dynamic quenching), formation of complexes in the ground state (static quenching), energy transfer, and charge transfer reaction.[29] To understand the mechanism in this case, we performed the well-known Stern−Volmer analysis (Figure 3a). The nonlinear nature of the plot

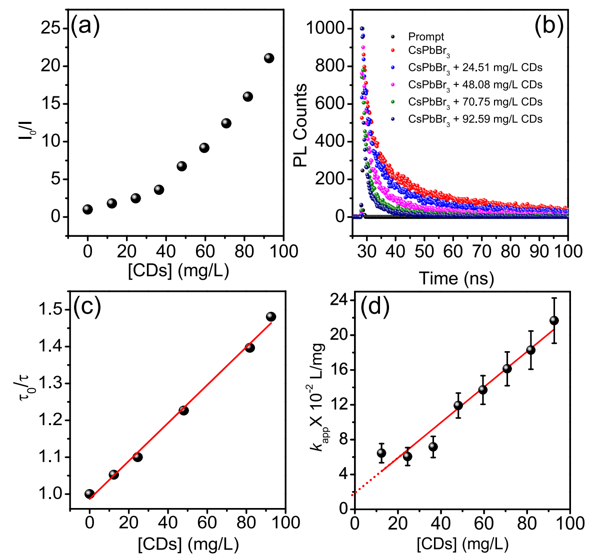

Figure 3. (a) Stern−Volmer plot for PL quenching of $CsPbBr_3$ NCs in the presence of varying concentrations of N-doped CDs. (b) Time-resolved PL spectra of 1.97×10^{-6} M $CsPbBr_3$NCs in toluene medium with different concentrations of N-doped CDs. (c) Stern−Volmer plot in terms of photoluminescence lifetime of $CsPbBr_3$ NCs in the presence of N-doped CDs. (d) Modified Stern−Volmer plot showing the variation of k_{app} as a function of the varying concentration of N-doped CDs.

follows the modified Stern−Volmer equation (eq 1), which shows an upward curvature due to the $[Q]^2$ term in eq 2.

$$\frac{I_O}{I} = (1 + k_S[Q])(1 + k_D[Q]) \tag{1}$$

$$\frac{I_O}{I} = 1 + (k_S + k_D)[Q] + k_S k_D [Q]^2 \tag{2}$$

$$\frac{I_O}{I} = 1 + k_{app}[Q] \tag{3}$$

$$k_{app} = k_S + k_D + k_S k_D [Q] \tag{4}$$

where I_O and I are the PL intensities of $CsPbBr_3$ NCs in the absence and presence of N-doped CDs, respectively, k_S and k_D are the static and dynamic quenching constants, respectively, and [Q] is the concentration of N-doped CDs.

This upward curvature might be attributed to the presence of both dynamic and static quenching mechanisms; thereby, we observe a decrease in PL intensity. Nevertheless, the measurement of the PL lifetime is more robust than the PL intensity as it depends on the intensity of excitation and not on the concentration in the $CsPbBr_3$−N-doped CD heterostructure system. Thus, we performed time-resolved PL spectroscopy. The PL decay of the $CsPbBr_3$−N-doped CD

https://dx.doi.org/10.1021/acs.jpclett.0c02139
J. Phys. Chem. Lett. 2020, 11, 8002−8007

heterostructure could be fitted with the use of multicomponent decay kinetics (Figure 3b), and the fitting parameters are listed in Table S1. The $CsPbBr_3$−N-doped CD heterostructure decayed relatively faster than pristine $CsPbBr_3$ with the average PL lifetime decreasing from 111.3 to 12.6 ns upon addition of a 92.59 mg/L CD solution (Figure 3b and Table S1). This difference between the τ_{avg} of the $CsPbBr_3$−N-doped CD heterostructure and that of pristine $CsPbBr_3$ indicates the origin of the nonradiative pathway from the substantial electronic interaction between $CsPbBr_3$ NCs and π electrons of N-doped CDs.[29] In the case of pure static quenching, the lifetime should be unaffected in the presence of N-doped CD quenchers. The slope of τ_o/τ with [Q] in Figure 3c gives a dynamic quenching constant (k_D) of 0.51 × 10^4 μL/mg via eq 5.

$$\frac{\tau_o}{\tau} = 1 + k_D[Q] \tag{5}$$

where τ_o and τ are the excited state lifetimes of $CsPbBr_3$ in the absence and presence of N-doped CDs, respectively. We have further estimated the static quenching constant, k_S, to be 1.32 × 10^4 μL/mg by plotting k_{app} with [Q] by using eqs 3 and 4 (see Figure 3d).

PL quenching is usually ascribed to either a nonradiative energy transfer or electron transfer mechanism. During the nonradiative energy transfer, generally the intensity of the donor emission decreases and that of the acceptor emission increases. As one can see in both Figure 2d and Figure S7, both $CsPbBr_3$ NC and N-doped CD emissions show decreases in intensity due to the lack of overlap between the emission spectra of $CsPbBr_3$ and CDs, which rules out the possibility of energy transfer.[29] Thus, photoinduced electron transfer from the photoexcited $CsPbBr_3$ NCs to N-doped CDs is the mechanism most likely to be involved in the quenching of the PL of the $CsPbBr_3$ NC. The photoexcited electrons can be injected from the $CsPbBr_3$ NC into the N-doped CD as it has an N-acceptor level. Subsequently, the band gap of $CsPbBr_3$ will decrease a bit, which is observed in the slight blue shift in PL (see Figure 2d). A similar blue shift of the PL of the electron donor was previously observed in $CsPbBr_3$−phosphorene and $CsPbBr_3$−MXene composites.[29,32]

To understand the electron transfer between N-doped CDs and $CsPbBr_3$ NCs, we estimated band edges by cyclic voltammetry as described in the Supporting Information. The onset reduction potentials were found to be −0.73 and −0.71 V for N-doped CDs and $CsPbBr_3$ NCs, respectively (Figure S8). The positions of the VB and CB levels of the $CsPbBr_3$ are at −6.06 and −3.69 eV, respectively, while for N-doped CDs, HOMOs are at −7.82 eV (π), −7.32 eV ($n_{C=O}$), and −5.99 eV ($n_{C=N}$) and the LUMO is at −3.67 eV (π^*) (see Figure 4a). It is well-known that N-doping in CDs introduces an acceptor state below the conduction band (as shown in Figure 4a),[43,44] which provides a quasi type II-like band alignment with the $CsPbBr_3$ NC.[59,60] Such trap states act as acceptor centers for electrons from the conduction band of $CsPbBr_3$.

To understand the charge transfer between the $CsPbBr_3$ NC and the N-doped CD, we have fabricated a photoconductivity device. From the current−voltage (I−V) measurement in the dark and in the presence of light (shown in panels b and c, respectively, of Figure 4), it is evident that the pure $CsPbBr_3$ NC shows a larger photocurrent enhancement due to the high absorption coefficient (931 cm^{-1} g^{-1} L) compared to that of the N-doped CD (low absorption coefficient of 22 cm^{-1} g^{-1} L), which has almost no photoresponse. In the $CsPbBr_3$−N-doped CD heterostructure, the photoexcited electrons from the $CsPbBr_3$ NC are trapped in the acceptor states of the N-doped CD (as shown in Figure 4a) and it becomes less available for photoconduction. This is evident from the decrease in photocurrent with an increase in the concentration of N-doped CDs (milligrams per liter) in the heterostructure system (Figure 4b,c).

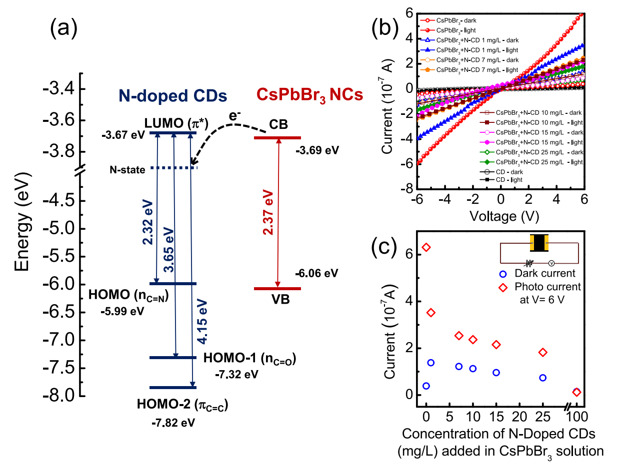

Figure 4. (a) Band energies of $CsPbBr_3$ NCs and N-doped CDs. (b) Current vs voltage (I−V) for $CsPbBr_3$ NCs with different concentrations of N-doped CDs under dark and illuminated conditions measured from −6 to 6 V. (c) Plot of the dark current and photocurrent of different concentrations of N-doped CDs (milligrams per liter) in 1.72 × 10^{-4} M $CsPbBr_3$. The inset shows the schematic device representation.

In summary, we have successfully demonstrated the heterostructure between $CsPbBr_3$ NCs and N-doped CDs, which exhibited PL quenching of the halide perovskite. N-Doping in the CD generated a trap state below the conduction band. The mechanism of PL quenching of $CsPbBr_3$ is charge transfer from the conduction band of the perovskite nanocrystal to the N-acceptor state of the CD arising because of quasi type II band alignment. The measured photoconductivity showed that the photocurrent decreases in the heterostructure system compared to that of $CsPbBr_3$ NCs as the photoexcited electrons from $CsPbBr_3$ are trapped in the N acceptor in the N-doped CDs. This work presents the synthesis and fundamental understanding of the charge transfer mechanism in the all-inorganic halide perovskite−carbon dot heterostructure, which will stimulate further research of new heterostructures with other halide perovskite and mixed-dimensional nanostructures.

■ ASSOCIATED CONTENT

Supporting Information

The Supporting Information is available free of charge at https://pubs.acs.org/doi/10.1021/acs.jpclett.0c02139.

Experimental Section and additional figures and tables (PDF)

■ AUTHOR INFORMATION

Corresponding Author

Kanishka Biswas − *New Chemistry Unit and School of Advanced Materials and International Centre for Materials*

https://dx.doi.org/10.1021/acs.jpclett.0c02139
J. Phys. Chem. Lett. 2020, 11, 8002−8007

Science, Jawaharlal Nehru Centre for Advanced Scientific Research (JNCASR), Bangalore 560064, India; orcid.org/0000-0001-9119-2455; Email: kanishka@jncasr.ac.in

Authors

Ekashmi Rathore − *New Chemistry Unit, Jawaharlal Nehru Centre for Advanced Scientific Research (JNCASR), Bangalore 560064, India*

Krishnendu Maji − *New Chemistry Unit, Jawaharlal Nehru Centre for Advanced Scientific Research (JNCASR), Bangalore 560064, India*

Dheemahi Rao − *Chemistry and Physics of Materials Unit, Jawaharlal Nehru Centre for Advanced Scientific Research (JNCASR), Bangalore 560064, India*

Bivas Saha − *Chemistry and Physics of Materials Unit and School of Advanced Materials and International Centre for Materials Science, Jawaharlal Nehru Centre for Advanced Scientific Research (JNCASR), Bangalore 560064, India*

Complete contact information is available at: https://pubs.acs.org/10.1021/acs.jpclett.0c02139

Notes

The authors declare no competing financial interest.

■ ACKNOWLEDGMENTS

K.B. acknowledges support from a Swarna-Jayanti fellowship, the Science and Engineering Research Board (SERB) (SB/SJF/2019-20/06), the Department of Science and Technology (DST) (DST/SJF/CSA-02/2018-19), and a Sheikh Saqr fellowship. E.R. and K.M. acknowledge Dr. Kaushik Kundu for discussions.

■ REFERENCES

(1) Kamat, P. V.; Pradhan, N.; Schanze, K.; Weiss, P. S.; Buriak, J.; Stang, P.; Odom, T. W.; Hartland, G. Challenges and opportunities in designing perovskite nanocrystal heterostructures. *ACS Energy Lett.* **2020**, *5*, 2253−2255.

(2) Stoumpos, C. C.; Kanatzidis, M. G. Halide perovskites: poor man's high-performance semiconductors. *Adv. Mater.* **2016**, *28*, 5778−5793.

(3) Protesescu, L.; Yakunin, S.; Bodnarchuk, M. I.; Krieg, F.; Caputo, R.; Hendon, C. H.; Yang, R. X.; Walsh, A.; Kovalenko, M. V. Nanocrystals of cesium lead halide perovskites ($CsPbX_3$, X = Cl, Br, and I): novel optoelectronic materials showing bright emission with wide color gamut. *Nano Lett.* **2015**, *15*, 3692−3696.

(4) Swarnkar, A.; Chulliyil, R.; Ravi, V. K.; Irfanullah, M.; Chowdhury, A.; Nag, A. Colloidal $CsPbBr_3$ perovskite nanocrystals: luminescence beyond traditional quantum dots. *Angew. Chem., Int. Ed.* **2015**, *54*, 15424−15428.

(5) Stranks, S. D.; Snaith, H. J. Metal-halide perovskites for photovoltaic and light-emitting devices. *Nat. Nanotechnol.* **2015**, *10*, 391−402.

(6) McCall, K. M.; Liu, Z.; Trimarchi, G.; Stoumpos, C. C.; Lin, W.; He, Y.; Hadar, I.; Kanatzidis, M. G.; Wessels, B. W. α-particle detection and charge transport characteristics in the $A_3M_2I_9$ defect perovskites (A = Cs, Rb; M = Bi, Sb). *ACS Photonics* **2018**, *5*, 3748−3762.

(7) Seth, S.; Ahmed, T.; De, A.; Samanta, A. Tackling the defects, stability, and photoluminescence of $CsPbX_3$ perovskite nanocrystals. *ACS Energy Lett.* **2019**, *4*, 1610−1618.

(8) Wu, Y.; Li, X.; Zeng, H. Highly luminescent and stable halide perovskite nanocrystals. *ACS Energy Lett.* **2019**, *4*, 673−681.

(9) Stoumpos, C. C.; Frazer, L.; Clark, D. J.; Kim, Y. S.; Rhim, S. H.; Freeman, A. J.; Ketterson, J. B.; Jang, J. I.; Kanatzidis, M. G. Hybrid germanium iodide perovskite semiconductors: active lone pairs, structural distortions, direct and indirect energy gaps, and strong nonlinear optical properties. *J. Am. Chem. Soc.* **2015**, *137*, 6804−6819.

(10) Slavney, A. H.; Hu, T.; Lindenberg, A. M.; Karunadasa, H. I. A bismuth-halide double perovskite with long carrier recombination lifetime for photovoltaic applications. *J. Am. Chem. Soc.* **2016**, *138*, 2138−2141.

(11) Kundu, K.; Acharyya, P.; Maji, K.; Sasmal, R.; Agasti, S. S.; Biswas, K. Synthesis and localized photoluminescence blinking of lead-free 2D nanostructures of $Cs_3Bi_2I_6Cl_3$ Perovskite. *Angew. Chem., Int. Ed.* **2020**, *59*, 13093−13100.

(12) Sarkar, A.; Acharyya, P.; Sasmal, R.; Pal, P.; Agasti, S. S.; Biswas, K. Synthesis of ultrathin few-layer 2D nanoplates of halide perovskite $Cs_3Bi_2I_9$ and single-nanoplate super-resolved fluorescence microscopy. *Inorg. Chem.* **2018**, *57*, 15558−15565.

(13) Tong, Y.; Bladt, E.; Aygüler, M. F.; Manzi, A.; Milowska, K. Z.; Hintermayr, V. A.; Docampo, P.; Bals, S.; Urban, A. S.; Polavarapu, L.; Feldmann, J. Highly luminescent cesium lead halide perovskite nanocrystals with tunable composition and thickness by ultrasonication. *Angew. Chem., Int. Ed.* **2016**, *55*, 13887−13892.

(14) Guria, A. K.; Dutta, S. K.; Adhikari, S. D.; Pradhan, N. Doping Mn^{2+} in lead halide perovskite nanocrystals: successes and challenges. *ACS Energy Lett.* **2017**, *2*, 1014−1021.

(15) Yang, D.; Cao, M.; Zhong, Q.; Li, P.; Zhang, X.; Zhang, Q. All-inorganic cesium lead halide perovskite nanocrystals: synthesis, surface engineering and applications. *J. Mater. Chem. C* **2019**, *7*, 757−789.

(16) Yakunin, S.; Protesescu, L.; Krieg, F.; Bodnarchuk, M. I.; Nedelcu, G.; Humer, M.; De Luca, G.; Fiebig, M.; Heiss, W.; Kovalenko, M. V. Low-threshold amplified spontaneous emission and lasing from colloidal nanocrystals of caesium lead halide perovskites. *Nat. Commun.* **2015**, *6*, 8056.

(17) Akkerman, Q. A.; D'Innocenzo, V.; Accornero, S.; Scarpellini, A.; Petrozza, A.; Prato, M.; Manna, L. Tuning the optical properties of cesium lead halide perovskite nanocrystals by anion exchange reactions. *J. Am. Chem. Soc.* **2015**, *137*, 10276−10281.

(18) Swarnkar, A.; Marshall, A. R.; Sanehira, E. M.; Chernomordik, B. D.; Moore, D. T.; Christians, J. A.; Chakrabarti, T.; Luther, J. M. Quantum dot-induced phase stabilization of α-$CsPbI_3$ perovskite for high-efficiency photovoltaics. *Science* **2016**, *354*, 92−95.

(19) Lin, H.; Zhou, C.; Tian, Y.; Siegrist, T.; Ma, B. Low-dimensional organometal halide perovskites. *ACS Energy Lett.* **2018**, *3*, 54−62.

(20) Novoselov, K. S.; Fal'ko, V. I.; Colombo, L.; Gellert, P. R.; Schwab, M. G.; Kim, K. A roadmap for graphene. *Nature* **2012**, *490*, 192.

(21) Rao, C. N. R.; Sood, A. K.; Subrahmanyam, K. S.; Govindaraj, A. Graphene: the new two-dimensional nanomaterial. *Angew. Chem., Int. Ed.* **2009**, *48*, 7752−7777.

(22) Liu, H.; Neal, A. T.; Zhu, Z.; Luo, Z.; Xu, X.; Tománek, D.; Ye, P. D. Phosphorene: an unexplored 2D semiconductor with a high hole mobility. *ACS Nano* **2014**, *8*, 4033−4041.

(23) Chhowalla, M.; Shin, H. S.; Eda, G.; Li, L.-J.; Loh, K. P.; Zhang, H. The chemistry of two-dimensional layered transition metal dichalcogenide nanosheets. *Nat. Chem.* **2013**, *5*, 263−275.

(24) Naguib, M.; Mochalin, V. N.; Barsoum, M. W.; Gogotsi, Y. MXenes: a new family of two-dimensional materials. *Adv. Mater.* **2014**, *26*, 992−1005.

(25) Tan, C.; Cao, X.; Wu, X.-J.; He, Q.; Yang, J.; Zhang, X.; Chen, J.; Zhao, W.; Han, S.; Nam, G.-H.; Sindoro, M.; Zhang, H. Recent advances in ultrathin two-dimensional nanomaterials. *Chem. Rev.* **2017**, *117*, 6225−6331.

(26) Geim, A. K.; Grigorieva, I. V. Van der Waals heterostructures. *Nature* **2013**, *499*, 419−425.

(27) Jariwala, D.; Marks, T. J.; Hersam, M. C. Mixed-dimensional van der Waals heterostructures. *Nat. Mater.* **2017**, *16*, 170−181.

(28) Banik, A.; Biswas, K. Synthetic nanosheets of natural van der Waals heterostructures. *Angew. Chem.* **2017**, *129*, 14753−14758.

(29) Muduli, S.; Pandey, P.; Devatha, G.; Babar, R.; M, T.; Kothari, D. C.; Kabir, M.; Pillai, P. P.; Ogale, S. Photoluminescence quenching

in self-assembled $CsPbBr_3$ quantum dots on few-layer black phosphorus sheets. *Angew. Chem.* **2018**, *130*, 7808−7812.
(30) Tang, X.; Zu, Z.; Zang, Z.; Hu, Z.; Hu, W.; Yao, Z.; Chen, W.; Li, S.; Han, S.; Zhou, M. $CsPbBr_3$/Reduced Graphene Oxide nanocomposites and their enhanced photoelectric detection application. *Sens. Actuators, B* **2017**, *245*, 435−440.
(31) Xu, Y.; Yang, M.; Chen, B.; Wang, X.; Chen, H.; Kuang, D.; Su, C. A $CsPbBr_3$ perovskite quantum dot/graphene oxide composite for photocatalytic CO_2 reduction. *J. Am. Chem. Soc.* **2017**, *139*, 5660−5663.
(32) Pan, A.; Ma, X.; Huang, S.; Wu, Y.; Jia, M.; Wangyang, P.; Liu, Y.; Shi, Y.; He, L.; Liu, Y. $CsPbBr_3$ perovskite nanocrystal grown on mxene nanosheets for enhanced photoelectric detection and photocatalytic CO_2 reduction. *J. Phys. Chem. Lett.* **2019**, *10*, 6590−6597.
(33) Ou, M.; Tu, W.; Yin, S.; Xing, W.; Wu, S.; Wang, H.; Wan, S.; Zhong, Q.; Xu, R. Amino-assisted anchoring of $CsPbBr_3$ perovskite quantum dots on porous g-C_3N_4 for enhanced photocatalytic CO_2 reduction. *Angew. Chem.* **2018**, *130*, 13758−13762.
(34) Ravi, V. K.; Saikia, S.; Yadav, S.; Nawale, V. V.; Nag, A. $CsPbBr_3$/ZnS core/shell type nanocrystals for enhancing luminescence lifetime and water stability. *ACS Energy Lett.* **2020**, *5*, 1794−1796.
(35) Liu, X.; Zhang, X.; Li, L.; Xu, J.; Yu, S.; Gong, X.; Zhang, J.; Yin, H. Stable luminescence of $CsPbBr_3$/nCdS core/shell perovskite quantum dots with al self-passivation layer modification. *ACS Appl. Mater. Interfaces* **2019**, *11*, 40923−40931.
(36) Brumberg, A.; Diroll, B. T.; Nedelcu, G.; Sykes, M. E.; Liu, Y.; Harvey, S. M.; Wasielewski, M. R.; Kovalenko, M. V.; Schaller, R. D. Material dimensionality effects on electron transfer rates between $CsPbBr_3$ and CdSe nanoparticles. *Nano Lett.* **2018**, *18*, 4771−4776.
(37) Zhang, X.; Wu, X.; Liu, X.; Chen, G.; Wang, Y.; Bao, J.; Xu, X.; Liu, X.; Zhang, Q.; Yu, K.; Wei, W.; Liu, J.; Xu, J.; Jiang, H.; Wang, P.; Wang, X. Heterostructural $CsPbX_3$-PbS (X = Cl, Br, I) quantum dots with tunable vis-nir dual emission. *J. Am. Chem. Soc.* **2020**, *142*, 4464−4471.
(38) Wang, S.; Bi, C.; Portniagin, A.; Yuan, J.; Ning, J.; Xiao, X.; Zhang, X.; Li, Y. Y.; Kershaw, S. V.; Tian, J.; Rogach, A. L. $CsPbI_3$/PbSe Heterostructured Nanocrystals for High-Efficiency Solar Cells. *ACS Energy Lett.* **2020**, *5*, 2401−2410.
(39) Li, H.; Kang, Z.; Liu, Y.; Lee, S. T. Carbon nanodots: Synthesis, properties and applications. *J. Mater. Chem.* **2012**, *22*, 24230−24253.
(40) Baker, S. N.; Baker, G. A. Luminescent carbon nanodots: emergent nanolights. *Angew. Chem., Int. Ed.* **2010**, *49*, 6726−6744.
(41) Pal, A.; Sk, M. P.; Chattopadhyay, A. Recent advances in crystalline carbon dots for superior application potential. *Mater. Adv.* **2020**, *1*, 525−553.
(42) Holá, K.; Sudolská, M.; Kalytchuk, S.; Nachtigallová, D.; Rogach, A. L.; Otyepka, M.; Zbořil, R. Graphitic Nitrogen Triggers Red Fluorescence in Carbon Dots. *ACS Nano* **2017**, *11*, 12402−12410.
(43) Sharma, A.; Das, J. Small molecules derived carbon dots: synthesis and applications in sensing, catalysis, imaging, and biomedicine. *J. Nanobiotechnol.* **2019**, *17*, 92.
(44) Dong, Y.; Pang, H.; Yang, H. B.; Guo, C.; Shao, J.; Chi, Y.; Li, C. M.; Yu, T. Carbon-based dots co-doped with nitrogen and sulfur for high quantum yield and excitation-independent emission. *Angew. Chem., Int. Ed.* **2013**, *52*, 7800−7804.
(45) Li, X.; Zhang, S.; Kulinich, S. A.; Liu, Y.; Zeng, H. Engineering surface states of carbon dots to achieve controllable luminescence for solidluminescent composites and sensitive Be^{2+} detection. *Sci. Rep.* **2015**, *4*, 4976.
(46) Qu, D.; Zheng, M.; Zhang, L.; Zhao, H.; Xie, Z.; Jing, X.; Haddad, R. E.; Fan, H.; Sun, Z. Formation mechanism and optimization of highly luminescent N-doped graphene quantum dots. *Sci. Rep.* **2015**, *4*, 5294.
(47) Choi, Y.; Kang, B.; Lee, J.; Kim, S.; Kim, G. T.; Kang, H.; Lee, B. R.; Kim, H.; Shim, S. H.; Lee, G.; Kwon, O. H.; Kim, B.-S. Integrative Approach toward Uncovering the Origin of Photoluminescence in Dual Heteroatom-Doped Carbon Nanodots. *Chem. Mater.* **2016**, *28*, 6840−6847.
(48) Li, Y.; Zhao, Y.; Cheng, H.; Hu, Y.; Shi, G.; Dai, L.; Qu, L. Nitrogen-Doped Graphene Quantum Dots with Oxygen-Rich Functional Groups. *J. Am. Chem. Soc.* **2012**, *134*, 15−18.
(49) Yeh, T. F.; Teng, C. Y.; Chen, S. H.; Teng, H. Nitrogen-Doped Graphene Oxide Quantum Dots as Photocatalysts for Overall Water-Splitting under Visible Light Illumination. *Adv. Mater.* **2014**, *26*, 3297−3303.
(50) Zhang, Y. Q.; Ma, D. K.; Zhang, Y. G.; Chen, W.; Huang, S. M. N-doped Carbon Quantum Dots for TiO_2-Based Photocatalysts and Dye-Sensitized Solar Cells. *Nano Energy* **2013**, *2*, 545−552.
(51) Wheeler, L. M.; Sanehira, E. M.; Marshall, A. R.; Schulz, P.; Suri, M.; Anderson, N. C.; Christians, J. A.; Nordlund, D.; Sokaras, D.; Kroll, T.; Harvey, S. P.; Berry, J. J.; Lin, L. Y.; Luther, J. M. Targeted Ligand-Exchange Chemistry on Cesium Lead Halide Perovskite Quantum Dots for High-Efficiency Photovoltaics. *J. Am. Chem. Soc.* **2018**, *140*, 10504−10513.
(52) Wang, S.; Du, L.; Jin, Z.; Xin, Y.; Mattoussi, H. Enhanced Stabilization and Easy Phase Transfer of $CsPbBr_3$ Perovskite Quantum Dots Promoted by High-Affinity Polyzwitterionic Ligands. *J. Am. Chem. Soc.* **2020**, *142*, 12669−12680.
(53) Peng, S.; Wei, Q.; Wang, B.; Zhang, Z.; Yang, H.; Pang, G.; Wang, K.; Xing, G.; Sun, X.; Tang, Z. Suppressing Strong Exciton-Phonon Coupling in Blue Perovskite Nanoplatelet Solids by Binary Systems. *Angew. Chem., Int. Ed.* **2020**, DOI: 10.1002/anie.202009193.
(54) Casalongue, H. S.; Kaya, S.; Viswanathan, V.; Miller, D. J.; Friebel, D.; Hansen, H. A.; Nørskov, J. K.; Nilsson, A.; Ogasawara, H. Direct observation of the oxygenated species during oxygen reduction on a platinum fuel cell cathode. *Nat. Commun.* **2013**, *4*, 2817.
(55) Chen, D.; Wu, W.; Yuan, Y.; Zhou, Y.; Wan, Z.; Huang, P. Intense multi-state visible absorption and full-color luminescence of nitrogen-doped carbon quantum dots for blue-light-excitable solid-state-lighting. *J. Mater. Chem. C* **2016**, *4*, 9027−9035.
(56) Dey, S.; Chithaiah, P.; Belawadi, S.; Biswas, K.; Rao, C. N. R. New methods of synthesis and varied properties of carbon quantum dots with high nitrogen content. *J. Mater. Res.* **2014**, *29*, 383−391.
(57) Michalet, X.; Pinaud, F. F.; Bentolila, L. A.; Tsay, J. M.; Doose, S.; Li, J. J.; Sundaresan, G.; Wu, A. M.; Gambhir, S. S.; Weiss, S. Quantum dots for live cells, in vivo imaging, and diagnostics. *Science* **2005**, *307*, 538−544.
(58) Cui, J.; Beyler, A. P.; Coropceanu, I.; Cleary, L.; Avila, T. R.; Chen, Y.; Cordero, J. M.; Heathcote, S. L.; Harris, D. K.; Chen, O.; Cao, J.; Bawendi, M. G. Evolution of the Single-Nanocrystal Photoluminescence Linewidth with Size and Shell: Implications for Exciton-Phonon Coupling and the Optimization of Spectral Linewidths. *Nano Lett.* **2016**, *16*, 289−296.
(59) Pavlopoulos, N. G.; Dubose, J. T.; Liu, Y.; Huang, X.; Pinna, N.; Willinger, M. G.; Lian, T.; Char, K.; Pyun, J. Type I vs. Quasi-Type II Modulation in CdSe@CdS Tetrapods: Ramifications for Noble Metal Tipping. *CrystEngComm* **2017**, *19*, 6443−6453.
(60) Teitelboim, A.; Meir, N.; Kazes, M.; Oron, D. Colloidal Double Quantum Dots. *Acc. Chem. Res.* **2016**, *49*, 902−910.

https://dx.doi.org/10.1021/acs.jpclett.0c02139
J. Phys. Chem. Lett. 2020, 11, 8002−8007